# Localized Phase Separation of Thermoresponsive Polymers Induced by Plasmonic Heating

Issei Aibara,[†,#] Jun-ichi Chikazawa, [†,#] Takayuki Uwada[‡] and Shuichi Hashimoto*[,†]

[†] Department of Optical Science and Technology, University of Tokushima, 2-1 Minami-Josanjima, Tokushima 770-8506, Japan.

[‡] Department of Chemistry, Josai University, 1-1 Keyakidai, Sakado, Saitama 350-0295, Japan.

Abstract

Optical excitation-induced heating of a single gold nanoparticle potentially offers a high-temperature field confined to the immediate neighborhood of the particle. In this study, we applied darkfield microscopy imaging and Rayleigh scattering spectroscopy to pursue phase separation of aqueous thermoresponsive poly(*N*-isopropylacrylamide) and poly(vinyl methyl ether) adjacent to a gold nanoparticle that was heated by continuous wave laser illumination. Gold nanoparticles were supported on transparent substrates of glass or sapphire. From the imaging study, we observed that a 1–10-μm microdroplet covering the nanoparticle formed and grew in time scales of seconds to a few tens of seconds. The growth was triggered by the illumination and the droplet collapsed when the laser was blocked. At the same time, we observed scattering spectral changes characterized by a progressive redshift in the localized surface plasmon resonance (LSPR) band and an increasing scattering intensity in wavelengths region shorter than the LSPR band with increasing laser intensity. The scattering spectral changes were interpreted by the encapsulation of the nanoparticle by a polymer-rich droplet with increasing sizes. The present study revealed that thermoresponsive polymers were attracted to a hot gold nanoparticle and formed a microdroplet under illumination with a wavelength near the LSPR. Our findings demonstrate the potential of plasmonic heating to manipulate polymer migration and accumulation, which may find applications in protein crystallization.

## Introduction

Thermoresponsive polymers represented by poly (*N*-isopropylacrylamide) (PNIPAM) exhibit phase separation (demixing) in aqueous solutions when heated above a critical temperature known as the lower critical solution temperature (LCST: $T_c$ = 32°C or 305 K).[1] This phenomenon has attracted much attention because of potential applications in drug delivery, separation and bio-switching.[2] The molecular mechanism of the phase separation is assumed to be a manifestation of a coil-globule transition followed by further aggregation, forming polymer-rich domains such as mesoglobules.[3] Intriguingly, such phase separation was induced locally using a focused near-infrared laser beam (focal spot diameter: ~1 μm, peak power density: ~$10^9$ W $cm^{-2}$, period: several minutes) with a wavelength of 1064 nm. The laser-illuminated aqueous PNIPAM and poly(vinyl methyl ether) (PVME) solutions resulted in a single microdroplet around the focal laser spot.[4-6] Here a high-temperature field created in water presumably confined the microdroplet by collecting the polymers, assisted by the optical force. This method has potential to create a droplet anywhere in a solution, if it can be prepared more quickly at much lower laser powers. Revealing liquid–liquid phase separation is also important in applications such as protein crystallization, which is assumed to proceed via a two-step process involving (1) the formation of liquid droplets of high protein concentration and (2) the generation of ordered protein clusters within the dense liquid intermediate prior to nucleation leading to protein crystals.[7-9] For thermoresponsive polymers, the dynamic growth process starts from the phase transition, then phase separation, leading to a microdroplet (Scheme 1) through local heating. This process has been poorly understood because of a lack of a proper means to observe submicrometer scale events, hampered by the resolution limit of optical microscopes. By confining heating to the nanoscale, assisted by a sensitive spectroscopic technique, we will be able to look into the detailed progress of temperature-induced phase separation.

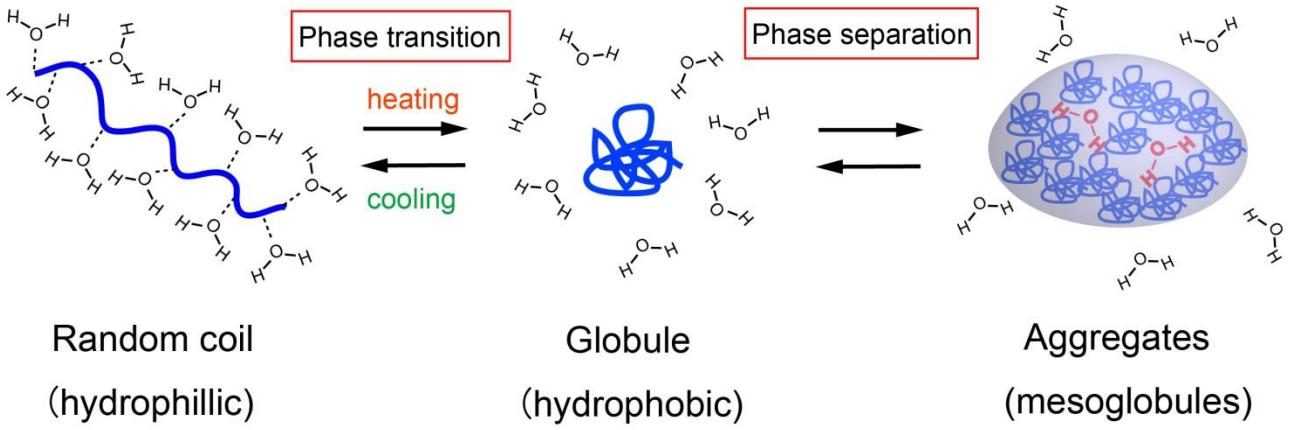


**Scheme 1**. Sketch of temperature-induced phase separation forming a polymer-rich domain via coil-to-globule phase transition.

---

Plasmonic nanoparticles (NPs) such as gold (Au) NPs have emerged as a nanoscale antenna that confines incident light in a subwavelength volume around the particle, thus tremendously concentrating the electric field.[10] This plasmonic field enhancement is the foundation for surface-enhanced Raman scattering and metal-enhanced fluorescence, both of which are promising for ultratrace analyses.[11,12] Simultaneously with the electric field enhancement, the light energy absorbed by the plasmonic NPs is efficiently converted into heat, raising the temperature of both the NP and the surrounding medium. This is referred to as the photothermal or plasmonic-heating effect.[13,14] Plasmonic heating is unique because only the medium immediately surrounding the NPs is heated by radial heat conduction, with the medium acting as an infinitely large heat sink. Thus the high-temperature field confined around the NP can be applied to drive the phase transition/phase separation of thermoresponsive polymers.

Such a possibility has been tested for PNIPAM very recently. Under a brightfield optical microscope, Orlishausen and Köhler observed the dynamic growth of PNIPAM aggregates that formed around laser-heated Au NPs.[15] The heating one of 250-nm-diameter Au NPs settled on a window in a 8–9 wt% PNIPAM solution with focused laser illumination at a constant power 51.9 mW (50–100 mW $\mu m^{-2}$ or $5 \times 10^6$–$10^7$ W $cm^{-2}$) and wavelength 532 nm enabled the growth of

phase-separated aggregates with diameters of ~10 μm at 0.3 s to ~100 μm at 500 s. Note here that the ranges of these laser powers well exceed the threshold of vapor bubble generation around a Au NP.[16-18] After laser heating was stopped, the aggregates dissolved from the outside. Because of a poor contrast of the brightfield method, early stages of aggregate formation were obscured. By using a 100-nm-diameter single Au NP under optical heating with low-intensity laser illumination ($10^4$–$10^5$ W $cm^{-2}$) combined with the Rayleigh light-scattering spectroscopy, Aibara and coworkers observed remarkable redshift in the localized surface plasmon resonance (LSPR) band of a Au NP exposed to aqueous PNIPAM solution.[19] This observation was ascribed to the plasmonic heating-induced nanoscale phase transition/separation to form PNIPAM aggregates within the high-temperature field surrounding the Au NP. This is distinct from the coil-to-globule volume phase transition of PNIPAM shell crosslinked around a Au NP core,[20-22] because PNIPAM molecules were not immobilized on the Au NP but were freely mobile in the solution. Although scattering spectroscopy is promising for revealing nanoscale events, laser intensity dependence has not been fully investigated for the LSPR spectral changes, and the particle temperature-dependent aggregation of PNIPAM to form a phase-separated droplet remains to be elucidated. There is still room to fill the gap between spectroscopic observations of plasmonic heating-induced PNIPAM phase transitions around Au NPs and microscope observations of PNIPAM-rich microdroplet formation.

The temperature field around the NP is not homogeneous but the temperature increases nearer to the NP surface.[18] Thus, the phase transition may start from the particle surface when the temperature exceeds the LCST at a certain threshold laser intensity, spreading from the surface to distant regions with increasing laser intensities. For experiments with medium water heating, a microdroplet with a diameter much greater than the heating laser spot size was formed after several minutes of exposure.[4-6] This may mean that PNIPAM molecules were transferred from outside the heating area to grow the droplet, although no detailed descriptions have been given. The transport and accumulation of colloids, cells and DNA exploiting optothermal manipulation through thermal

and Marangoni convections and thermophoresis are currently under intense investigation.[23-29] These studies used substrates with a thin Au layer or a Au nano-island film for heating effectively with a focused laser. Nevertheless, the heat transfer is complex, making temperature analysis difficult. In contrast, single Au NP heating is expected to yield a much simpler temperature field around the Au NP. Thus, the transport mechanism can be simplified. Moreover, in terms of their varying thermal conductivities, substrates play a decisive role in controlling particle temperature and temperature gradient at particle–medium and particle–substrate interfaces, promoting accumulation.[30]

In the present study we used darkfield microscopy-based imaging and light-scattering spectroscopy of a single Au NP to reveal a dynamic picture of phase separation for thermoresponsive polymers induced by single-particle plasmonic heating. Because of light scattering, the darkfield microscopy imaging can offer high-contrast images against a dark background for small objects that are otherwise difficult to view. We looked into the effect of different substrates on transport properties of such polymers. We show that plasmonic heating has a clear advantage over optical trapping to drive these polymers for manipulation with a significantly lower power.

**Experimental Methods**

*Experimental Setup*: The outline of the present experiment is shown in Scheme 2a, with an experimental setup given in Scheme 2b. The darkfield imaging was performed on an inverted optical microscope, IX-71 (Olympus, Tokyo, Japan; with a darkfield condenser NA = 0.8–0.92) equipped with a DS-5M digital camera (Nikon, Tokyo, Japan). The single-particle scattering spectra were recorded with a wavelength resolution of 0.5 nm on a spectrophotometer consisting of a SP-300*i* polychromator (Acton Research Co. MA) with a grating of 150 or 300 grooves/mm blazed at 500 nm and a DU401-BR-DD CCD camera (Andor Technology, Belfast, UK; operated at −60°C) through a 500-μm-diameter pinhole (view area: 10-μm diameter). A halogen lamp with a broad (white) spectrum was used for illumination when recording the scattering images and spectra. The spectra were obtained by subtracting the background signals including Raman scattering of the surrounding media and photoluminescence of the NP, then dividing it by the spectral profile of the white-light excitation source. A HA50 IR-cut filter (Hoya Candeo Optronics, Tokyo, Japan) was used for minimizing the lamp heating. Single Au NPs adsorbed on the top wall (ceiling) of the chamber (see Scheme 2b) were heated by illuminating a focused 488-nm CW laser, OBIS-488-LX-150 (Coherent, Santa Clara, CA) beam through a microscope objective (60×, NA = 0.70). We used a 488-nm wavelength laser for a few reasons. (1) The scattering spectra of nominal 100-nm-diameter Au NPs extend from 500 to 800 nm; hence, we did not use a 532 nm laser for excitation to avoid the superposition of a strong excitation light on relatively weak scattering spectra. (2) The excitation wavelength of 488 nm is slightly off-set from the LSPR peak position and the absorption cross-section, $C_{abs}$, is then unaffected by temperature changes. In contrast, the LSPR peak intensity is strongly dependent on particle temperature and changes in medium refractive index.[16] The excitation of the LSPR band causes the value of $C_{abs}$ for NPs to decrease with increasing temperature because of the temperature-induced damping, making estimates of the particle temperature difficult. (3) At the excitation wavelength of 488 nm, no light absorption and subsequent temperature increase are expected for glass, sapphire, PNIPAM, and PVME. The 488

nm laser light excites both interband and intraband transitions. Note, however, that the consequence of both excitations is the same: hot electron generation and subsequent particle heating.[32] The temperature increase of an Au NP occurs simultaneously with opening the shutter and the temperature decrease follows immediately after closing the shutter.[33] The spatial laser profile was determined by measuring scattering signal intensity of the 100-nm-diameter Au NP while scanning the stage at 100-nm interval. The FWHM of the laser beam thus determined was 0.6 μm. The laser peak power density $I_p$ (mW $\mu m^{-2}$) was represented by $I_p = [P(2.3546)^2]/[2\pi(FWHM)^2]$,[31] where $P$ is the laser power density (measured laser power divided by beam area). The irradiation periods were regulated using an F77 mechanical shutter (Suruga Seiki, Tokyo, Japan). All measurements were performed at 24±1°C.

*Sample preparation*: Poly (*N*-isopropylacrylamide) (PNIPAM, $M_w$ = 30,000) was obtained from Sigma-Aldrich Co.(St. Louis, MO) while poly(vinyl methyl ether) (PVME, 30% in water, $M_w$ = 47,000) was from Tokyo Kasei Co (Tokyo, Japan). The structural formulas of PNIPAM and PVME were given in Scheme 2c. Aqueous solutions of Au NPs with nominal diameters of 100 nm (EMGC100) were obtained from BBI Solutions, Cardiff, UK. Au NPs were transformed from faceted to spherical shape by irradiating with weak-intensity nanosecond laser pulses (~11 mJ $cm^{-2}$) of 532-nm wavelength. The particle image acquired using a transmission electron microscope and the corresponding size distribution (102±5 nm) are given in the Supporting Information, S1. Spherical Au NPs were spin-coated onto the 0001 face of an optically polished sapphire substrate (Shinkosha, Yokohama, Japan) of size 15 mm × 15 mm × 0.3 mm or a borosilicate cover glass (Matsunami, Osaka, Japan) of 24 mm × 32 mm × 0.17 mm. The Au NPs were washed twice with double-distilled water by placing 0.5 mL of water on a spin coater and spun. Au NPs were immersed in solutions of PNIPAM and PVME in an 11-μL chamber consisting of a sapphire/glass substrate, a 0.2-mm-thick silicon rubber spacer, and a 24 mm × 32 mm × 0.17 mm microscope cover slip. The substrates were cleansed in a boiling mixture of 1:1 30% $H_2O_2$ - 28% ammonia

mixture for 90 min, and plasma-cleaned in a YHS-R reactor (70 W, 20 kHz; Sakigake Semiconductor, Kyoto, Japan) for 60 s just before use.

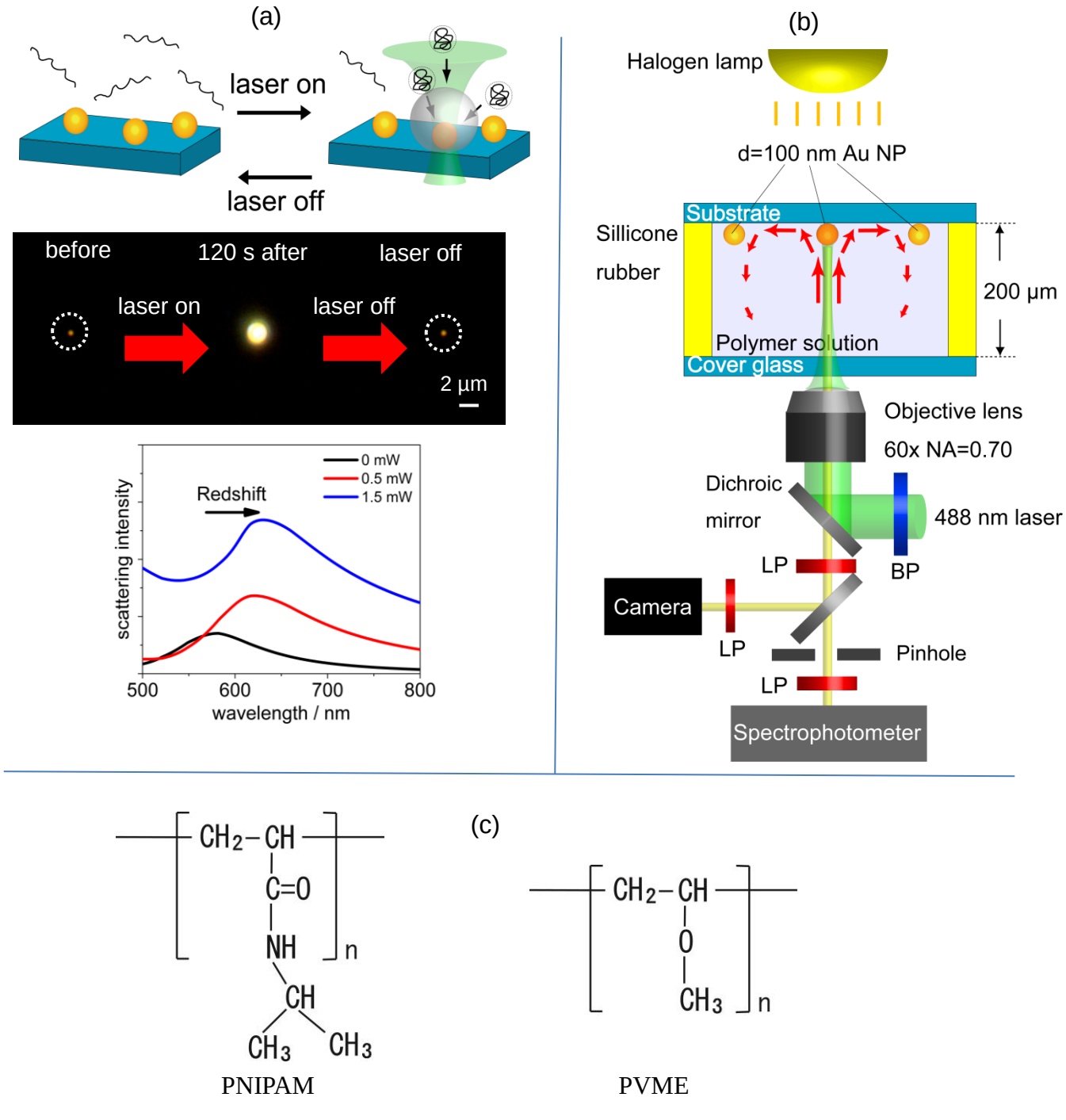


**Scheme 2**. Experimental overview. (a) upper: pictorial representation of the event, i.e. phase separation of the thermoresponsive polymers on plasmonic-heating, middle: darkfield microscopy images showing a transition of a single Au NP on exposure to laser illumination in aqueous solution of a thermoresponsive polymer, and lower: Rayleigh light scattering spectral changes of a single Au NP at various laser intensities. (b) experimental setup consisting of a chamber-structured specimen, a darkfield illumination system, a microscope objective, an excitation laser, a digital camera, and a CCD spectrophotometer. BP: laser line filter, LP: long-pass filter. (c) Structural formulas of poly(*N*-isopropylacrylamide) (PNIPAM) and poly(vinyl methyl ether) PVME.

## Results and Discussion

*1. Temperature distributions around a single Au NP*

When a Au NP supported on a substrate is subjected to laser illumination, particle heating occurs instantaneously, followed by heat transfer to the surroundings.[33] Using COMSOL Multiphysics, we simulated the two-dimensional (2D) temperature distribution around a Au NP under steady-state laser illumination. We considered both thermal and Marangoni convections initiated by medium heating in addition to radial heat conduction into both the substrate and the medium.[26-28] This is because Marangoni convection is driven by the temperature-dependent interfacial (liquid–solid) tension gradient as well as surface (liquid–air) tension gradient.[34] The numerical analysis of such flows have been performed previously for bubble-induced thermal and Marangoni convections.[35] Figure 1 a and b shows the simulated temperature map at a prototypical laser peak power density for two substrates, glass and sapphire, with notably differing thermal conductivities. Because of higher thermal conductivity, the sapphire substrate has a remarkable cooling effect. As a result, the particle temperature is lower for the system with sapphire (sapphire/water). For instance, the input laser intensity in Figure 1a is 20% of that in Figure 1b. Nevertheless, the calculated particle temperatures are nearly the same. Most notably, the convections create horizontally-expanded isothermal distributions that were not seen without such convections.[30] This is because the calculated convective flow rates represented by the arrow lengths suggest that flow rates in glass/water are much higher than those in sapphire/water at a given particle temperature. By increasing laser power, the high-temperature area expanded much greater than the area adjacent to the particle with a diameter of 100 nm.

Figure 1c depicts the laser peak power density vs. particle temperature curves for sapphire/water and glass/water systems. As seen from the figure, the particle temperature in glass/water is always much higher than that in sapphire/water at the same laser intensity.

(a)

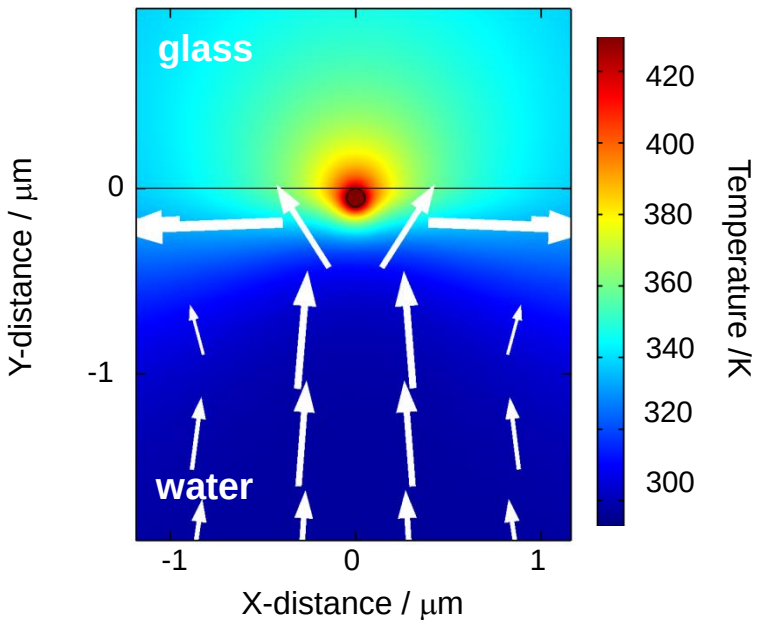
glass
water
Y-distance / μm
X-distance / μm
Temperature /K
420
400
380
360
340
320
300
0
-1
1

(b)

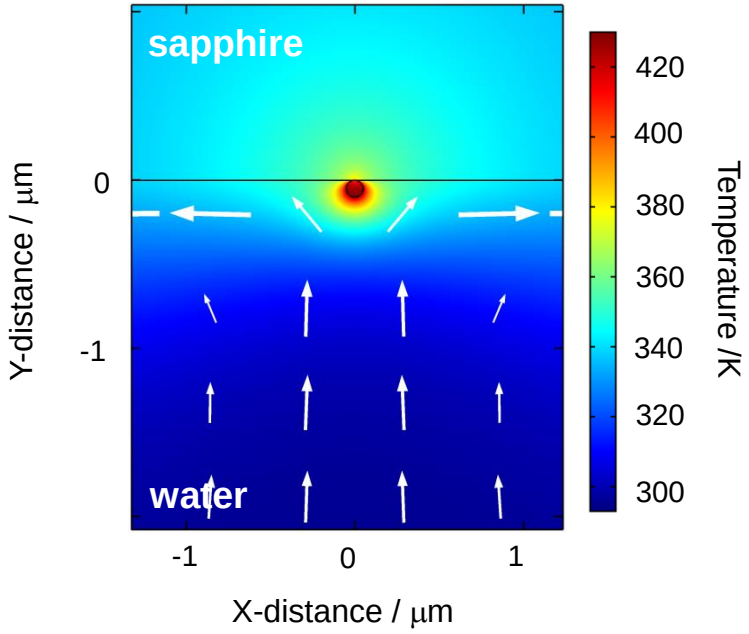
sapphire
water
Y-distance / μm
X-distance / μm
Temperature /K
420
400
380
360
340
320
300
0
-1
1

(c)

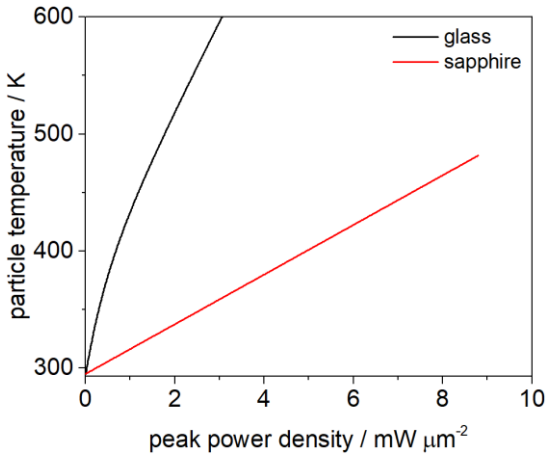
glass
sapphire
particle temperature / K
peak power density / mW μm-2
600
500
400
300
0
2
4
6
8
10

**Figure 1**. Simulated 2D temperature distributions for a single water-immersed 100-nm Au NP on glass (a, 1.0 mW $\mu m^{-2}$) and on sapphire (b, 5.3 mW $\mu m^{-2}$), under optical illumination from a CW laser. The length of white arrows corresponds to the magnitude of the convective flow rates. (c) Calculated particle temperature as a function of applied laser peak power density for a water-immersed 100-nm-Au NP on sapphire (red line) and glass (black line) substrates. Note that the water temperature is the same as the particle temperature at the NP surface. To calculate temperature, we used the thermal conductivity of water because the PNIPAM contribution is minor. Thermal conductivities used for calculation: water, 0.60 W $m^{-1}$ $K^{-1}$; borosilicate glass (D263T), 1.0 W $m^{-1}$ $K^{-1}$; sapphire, 41 W $m^{-1}$ $K^{-1}$. The temperature simulation was performed for laser intensities that may not exceed the bubble formation threshold.

---

The nonlinear temperature increase was remarkable in glass/water because of the higher temperatures that induced higher convection rates. With both different substrates, the high-temperature region increased in area with increasing laser intensity. From the particle temperature as a function of laser peak power density given in Figure 1c, the threshold of bubble formation can occur at ~3 mW $\mu m^{-2}$ for glass/water system. On the other hand, it is estimated at > 10 mW $\mu m^{-2}$ for sapphire/water system. Next, we will show the experimental evidence of phase separation, in which the particle temperature and the medium temperature distribution play a major role.

*2. Microscopy imaging on plasmonic heating.*

Darkfield microscopy imaging of a single Au NP was performed coupled with plasmonic heating in aqueous solutions of thermoresponsive polymers, depending on polymer concentration and laser intensity. Upon laser illumination of a 100-nm Au NP supported on a glass substrate and submerged in aqueous PNIPAM solution, we observed the formation and growth of a light-scattering sphere (2D images) centered at the position of the Au NP subjected to illumination. Figure 2 a and b shows images captured by a digital camera (the corresponding movie files, Movies 1-4 can be found in the Supporting Information); a and b compare the cooling effect of different substrates on plasmonic heating. In Figure 2a, a scattering sphere immediately grows to diameter > 2 μm within 5 s of illumination and exhibits a very slow growth to diameter ~2 μm (see $t_2$ = 10 to $t_5$ = 120 s). The brightfield image of a scattering sphere (Figure 2c, I and Supporting Information S2) shows a transparent planoconvex lens-like shape suggesting a droplet formed. It has been found that gel-like PNIPAM-rich agglomerates grow within the phase-separating solutions upon heating homogenous PNIPAM solutions across $T_c$.[36-38] However, the single-domain phase separation occurred for local heating;[4-6] plasmonic-heating-induced droplet formation encapsulating the Au NP, as demonstrated here, is unprecedented. The observed diameter of a light-scattering sphere as a function of illumination period at laser peak power densities of 0.7–2.6 mW $\mu m^{-2}$ is given in Supporting Information S3 (below 0.7 mW $\mu m^{-2}$, we had experimental difficulty in imaging hampered by an illuminating laser spot as will be explained below). We clearly observed the formation of a scattering entity at ~0.7 mW $\mu m^{-2}$ on a glass substrate. When the laser light is blocked after 120 s of illumination, the scattering sphere collapsed immediately (see $t_1$ (off) = 0.25 to $t_3$ (off) = 55 s) and the original Au NP image recovered. The single-particle light-scattering spectra of Au NP at $t_1$ and t (off) are nearly the same, suggesting that original bare Au NP was reproduced after illumination was terminated.

(a)

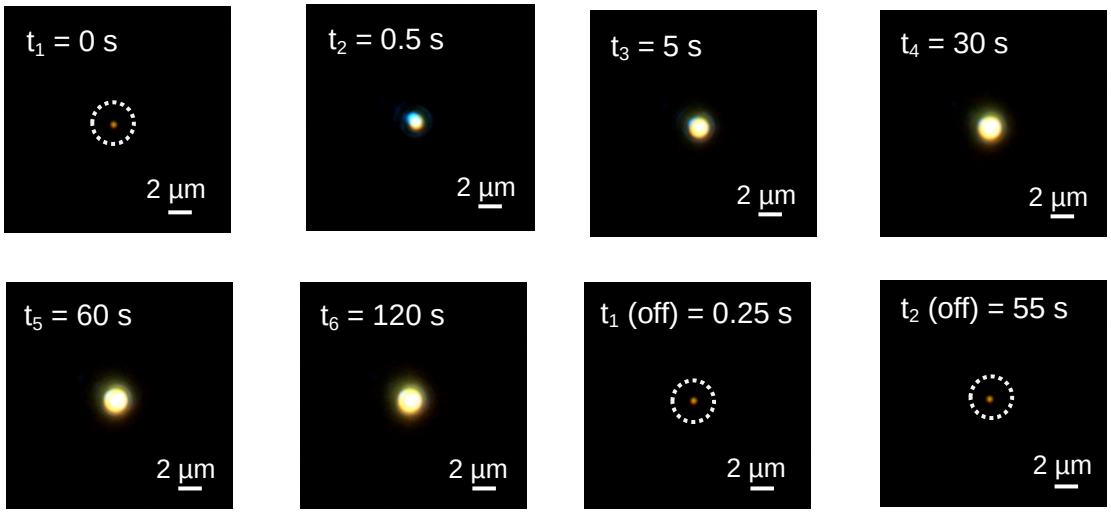
t1 = 0 s
2 µm
t2 = 0.5 s
2 µm
t3 = 5 s
2 µm
t4 = 30 s
2 µm
t5 = 60 s
2 µm
t6 = 120 s
2 µm
t1 (off) = 0.25 s
2 µm
t2 (off) = 55 s
2 µm

(b)

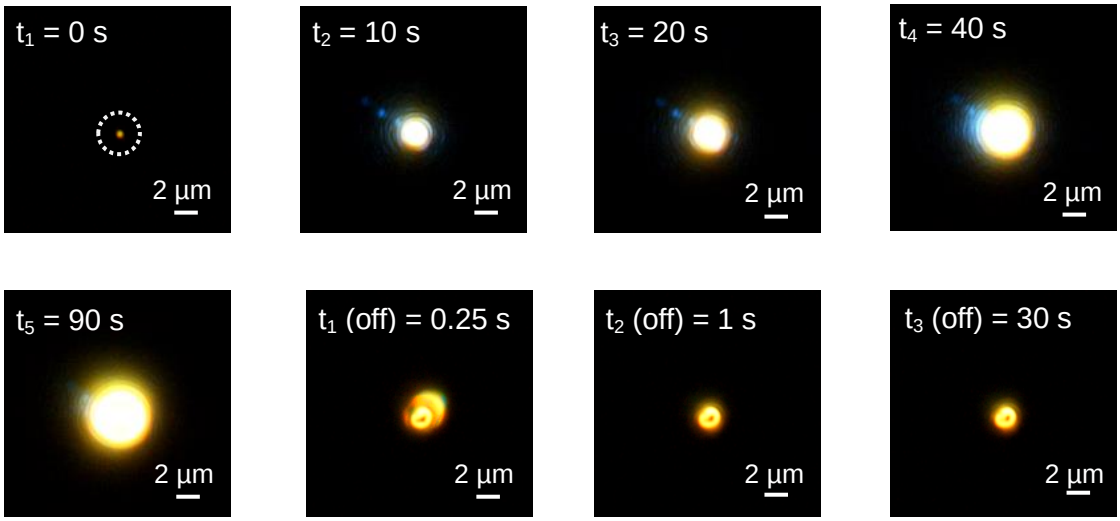
t1 = 0 s
2 µm
t2 = 10 s
2 µm
t3 = 20 s
2 µm
t4 = 40 s
2 µm
t5 = 90 s
2 µm
t1 (off) = 0.25 s
2 µm
t2 (off) = 1 s
2 µm
t3 (off) = 30 s
2 µm

(c)

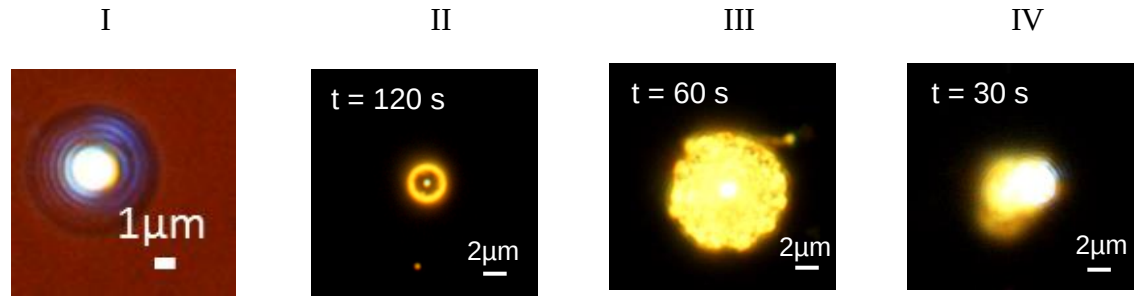
I
II
III
IV
1µm
t = 120 s
2µm
t = 60 s
2µm
t = 30 s
2µm

(d)

I II III

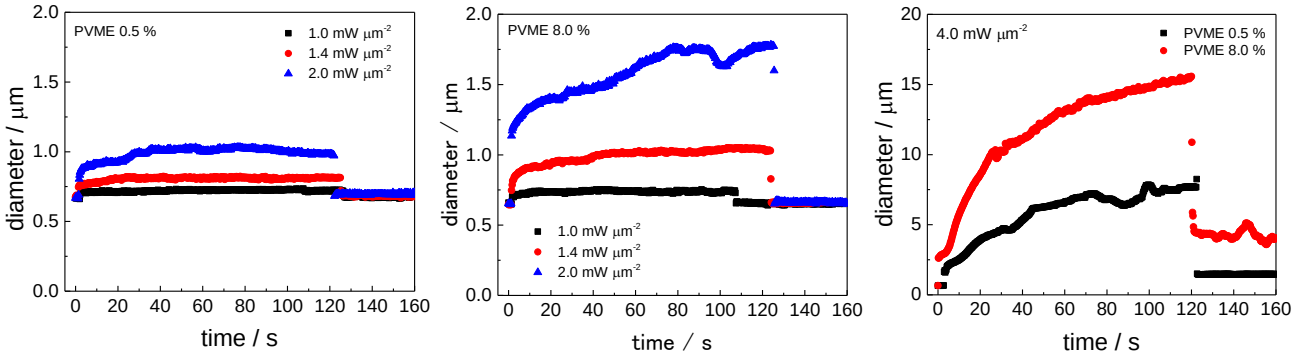


**Figure 2**.

(a, b) Darkfield light-scattering images representing time evolution starting from the excitation of a single 100-nm-diameter Au NP supported on a glass substrate (a, 1.8 mW $\mu m^{-2}$) or a sapphire substrate (b, 5.3 mW $\mu m^{-2}$), submerged in aqueous 0.96% PNIPAM solution.

(c) Magnified images: I, brightfield image of 200-nm-diameter Au NP. The particle was exposed to laser irradiation at 5.3 mW $\mu m^{-2}$ for 190 s; II, darkfield image showing a bright spot at the Au NP surrounded by dark and bright concentric rings; III, darkfield image of a rapidly growing bright scatterer consisting of very small scatterers; and IV, darkfield image showing a moving scatterer. In II–IV, 100-nm-diameter Au NP s were exposed to laser irradiation (laser peak power density: II. 1.8 mW $\mu m^{-2}$; III. 5.3 mW $\mu m^{-2}$; IV. 3.5 mW $\mu m^{-2}$) for periods given in the images. The particles are supported on a glass substrate and submerged in 0.96% PNIPAM solution.

(d) Light-scattering sphere diameter as a function of time from the start of laser illumination on the 100-nm-diameter Au NP at various laser intensities and concentrations of PVME; I: 0.5% PVME, II: 8.0% PVME, III: laser intensity 4.0 mW $\mu m^{-2}$ for 0.5% PVME and 8.0% PVME.

The observed diameters of 100-nm Au NPs on a digital camera are 0.7–0.8 μm because of the diffraction limited optics.

---

This result suggests that the phase separation of PNIPAM reversibly forms a microdroplet around Au NP in response to the particle temperature increase/decrease. That is, the particle temperature and resultant temperature distribution around the Au NP, given in Figure 1 a and b, are decisive for the size and shape of phase-separated droplets because the droplets formed are in dynamic equilibrium with incoming and outgoing molecules. As a result, steady-state droplet diameter that depends on the illumination intensity was reached as time proceeded (Figure 2a and Supporting Information, Figure S3a).

Light-scattering imaging relies on the distinct difference in refractive indices, so the clear boundary that occurred between the domain and the medium suggests that the domain has a much greater refractive index than water, indicative of phase separation. Indeed, the refractive index of n=1.495[39] reported for pure amorphous PNIPAM is considerably higher than that of water, n=1.333 at ambient temperature. The phase separation results in polymer-rich domain containing water, the amount of which is inaccessible. Therefore the refractive index of PNIPAM-rich droplet can be smaller than that of neat polymer.

Figure 2b shows the time evolution of light-scattering images for a sapphire substrate. Formation of a scattering sphere similar to those observed on a glass substrate occurred, but at much higher laser intensities > ~ 3 mW $\mu m^{-2}$. Below this intensity, the illuminating laser spot hampered the imaging of PNIPAM-rich droplet, although the laser was attenuated by blocking with a filter before the camera. Minimum intensity was necessary to locate the beam position to irradiate the Au NP, however. The higher threshold of droplet formation can be ascribed to greater cooling effect of a sapphire substrate caused by much larger thermal conductivity as discussed in the previous section. With the lapse of time, a gradual increase in the diameter of a scattering sphere occurred until 120 s reaching a diameter of 4.5 μm. The slower droplet growths observed in sapphire/water system can be ascribed to lower flow rates and greater deviation from centrosymmetric temperature distribution around the particle, estimated for the system than the glass/water system (compare Figure 1, a and b). On blocking the laser light, however, a

phenomenon distinct from that observed on a glass substrate occurred. The scattering images without laser illumination were appreciably greater in size than those of the original Au NP. In this case, a fixation of polymer around the Au NP resulted. The detailed account of this observation is given in section 4.

In addition to PNIPAM, we applied the darkfield imaging technique to monitor the plasmonic-heating-induced phase separation of aqueous PVME, which is also known for its thermoresponsive nature.[40-42] Figure 2d was constructed based on the scattering sphere diameter dependent on illumination time (see Supporting Information S4 for images). In this case, clear laser-power-dependent diameter growth was observed on a glass substrate in the range of laser powers we used (I and II). Notably the time-dependent diameter growth was concentration dependent; at 0.5% PVME, a fast growth occurred within 2 s, which is similar to the observation for PNIPAM. At 8.0%, however, a slow growth from 5 to 50 s occurred. This concentration dependence is safely ascribed to the effect of higher viscosity that gives reduced diffusion coefficients for polymers at higher concentrations (Supporting Information S5). At higher laser powers, a remarkably steeper diameter increase with time occurred, which is also dependent on the PVME concentration. Such an example at 4.0 mW $\mu m^{-2}$ is given in Figure 2d III. At 8.0% PVME, the diameter growth occurred immediately. Furthermore, after terminating the laser illumination, an increased particle diameter of 1.5 μm at 8.0% PVME was observed. This diameter increase after illumination was only observed at laser intensities > 4.0 mW $\mu m^{-2}$. The observations of remarkably steep diameter rise and permanent fixation at high intensities strongly suggest that bubble formation occurred because of strong heating.[26-29,35] Presumably, the higher PVME concentration acted to induce bubble generation. Permanent fixation on glass substrates was also observed for PNIPAM at high laser intensities (Supporting Information, Figure S3b).

Finally, we comment on the shape of light scatterers: phase-separated droplets. As shown in Figure 2 a and b, the light scatterers exhibited basically plain spherical shapes of various diameters. In contrast, when the laser power was increased to 1.8 mW $\mu m^{-2}$, we could see ring structures as

shown in Figure 2c, II. The central bright spot is ascribed to the location of a hot Au NP where the light-scattering intensity can be very high because such a high temperature attracts and concentrates PNIPAM molecules to a greater extent. The peripheral ring also exhibited high scattering intensity. On this occasion, we ascribe the ring observation to purely optical effect: the outside of a droplet is bright because of the difference in the refractive index of PNIPAM-rich domain from that of water at a focus while the inside is dark because of a droplet size exceeding the Rayleigh length of the optics. In fact, brightfield images gave no such rings. At a much higher intensity of 5.3 mW $\mu m^{-2}$, we observed a very bright droplet growing rapidly. In this case, a droplet is regarded as the assembly of small grains that scatters light efficiently, Figure 2c, III. We occasionally observed rotating scatterers as shown in Figure 2c, IV. In such cases, one side of the scatterer was observed to rotate around a sphere (see Movie 5). These dynamic features of scatterers are indicative of the formation of droplet through plasmonic heating-induced phase separation.

*3. Plasmonic-heating-induced LSPR scattering spectral shifts*

Figure 3a shows the Rayleigh scattering spectral changes of a 100-nm-diameter Au NP submerged in aqueous 1.0% PVME solution, before, during, and after illumination. In this experiment, Au NPs were supported on a glass substrate. For the scattering spectra, redshift occurred only during illumination; when the illumination stopped, the original spectra returned. The spectral shift was dependent on the laser intensity: the spectral shift was within experimental error at a laser peak power density of 0.10 mW μm$^{-2}$ (1.0 × 10$^4$ W cm$^{-2}$), whereas appreciable redshifts of 13 nm at 0.30 mW μm$^{-2}$ and 54 nm at 0.50 mW μm$^{-2}$ were recorded. The LSPR scattering spectral peak shift was plotted as a function of laser peak power density in Figure 3b, showing progressive redshift with increase in laser intensity.

---

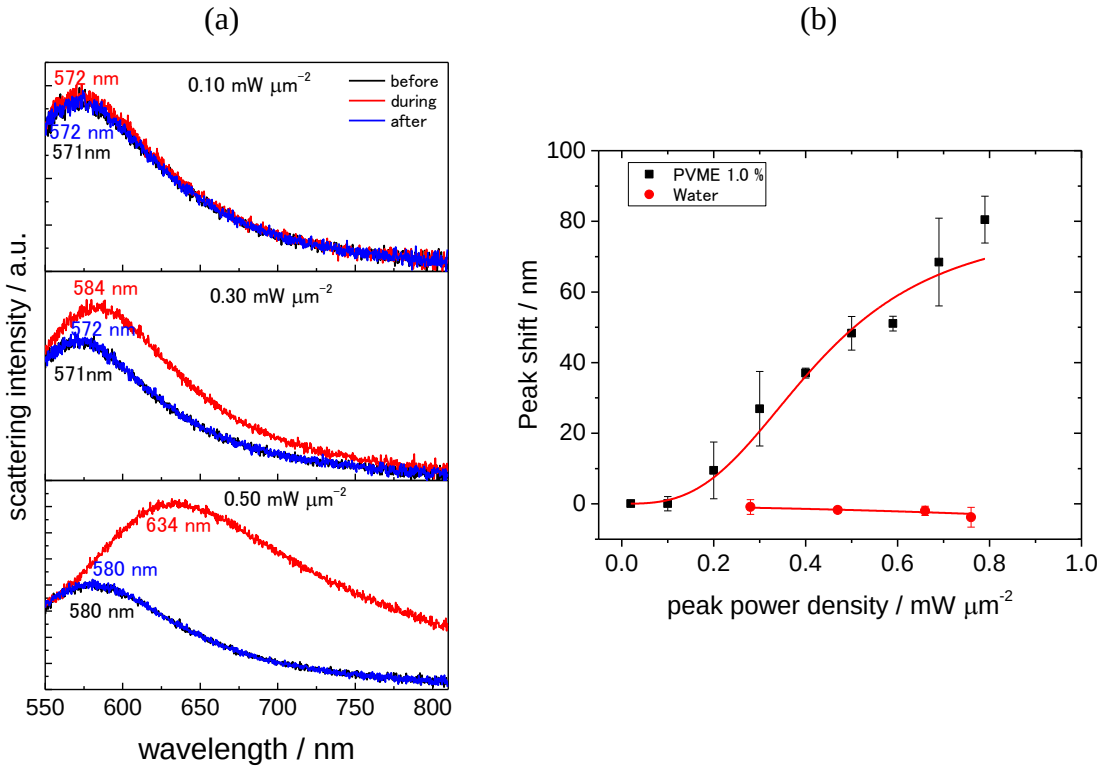


**Figure 3**. *In situ* scattering spectral changes: before, during, and after laser illumination of a 100-nm-diameter Au NP supported on a glass substrate and submerged in aqueous solution of 1.0% PVME: (a) scattering spectra during the illumination of 488-nm laser light at laser peak power densities, 0.10, 0.30 and 0.50 mW μm$^{-2}$, together with spectra before and after irradiation, (b) scattering spectral peak shift as a function of laser peak power density. 1.0 mW μm$^{-2}$ = 10$^5$ W cm$^{-2}$ = 10$^9$ W m$^{-2}$.

The observation of LSPR redshift of a single Au NP in aqueous PVME is similar to a previous observation in aqueous PNIPAM solution.[19] The origin of the spectral shift was ascribed to a LCST-induced aggregation of PNIPAM around the NP through heating of the surrounding medium with heat transfer from the optically heated NP. PNIPAM molecules are hydrophilic at temperatures below LCST (305 K), but hydrophobic above LCST.[1,3] The aggregated PNIPAM around a Au NP was assumed to increase the refractive index of the medium sensed by the Au NP, resulting in LSPR scattering redshift.[19] Aqueous PVME solution exhibits thermoresponsive nature with a LCST at around 308 K.[6, 39-41] The present results showed that the scattering spectral peak shift continued to increase as the laser intensity increased (Figure 3b). At the same time, the imaging study (Figure 2) revealed microdroplets formed surrounding the Au NP at intensities higher than those used in the scattering spectroscopic studies. These results suggest that the droplet size of phase-separated polymer aggregates increases as the particle temperature increases. Our findings revealed that PVME, as well as PNIPAM, underwent plasmonic-heating-induced phase separation, forming a droplet. Next, we attempt to estimate the size of phase-separated droplets below the diffraction-limited size from the scattering spectral changes. This may compliment the imaging study, which is only applicable to size estimation of droplets > 1 μm.

Figure 4 a and b shows the laser intensity-dependent scattering spectral changes of a Au NP under laser illumination in aqueous PNIPAM solutions at two concentrations, 0.48% (Figure 4a) and 0.96% (Figure 4b). In this experiment, 100-nm-diameter Au NPs were supported on a sapphire substrate. We used a wide range of excitation intensities, peak power density < 2.6 mW $\mu m^{-2}$, for which reversible redshift of the LSPR scattering spectra occurred. For imaging studies in section 2, we used much higher intensities: 5.3–8.8 mW $\mu m^{-2}$. In Figure 4a, besides the redshift, increased spectral bases are exhibited at lower wavelengths near 500 nm for illumination at high intensities. The increased bases are more pronounced in Figure 4b, in which twice the higher concentration of PNIPAM than that in Figure 4a is used. Here, a remarkable increase in the spectral bases occurred, in particular at shorter wavelengths, as the laser intensity increased. This is typical for Rayleigh

scattering, the intensity of which has $\lambda^{-4}$-dependence, from a non-absorbing particle, the refractive index of which is greater than that of the medium.[43] We checked that this increased scattering base was not an artifact caused by stray laser light: a combination of laser band-pass and long-pass filters effectively blocked the excitation light, whereby the observation of the scattering spectra below 500 nm was hampered. The observed scattering spectral changes, both LSPR redshift and increased base in particular at lower wavelength, were interpreted by encapsulation of Au NP in a polymer droplet, the thickness of which increases depending on the laser intensity and polymer concentration. As shown in Figure 4c, the LSPR scattering peak redshift started at an intensity of 0.25 mW $\mu m^{-2}$ and continued without saturation nearly independent of PNIPAM concentration. This may suggest that the size of the droplet encapsulating the Au NP depends largely on the NP temperature.

To assess the effect of encapsulation on the scattering spectral changes, we performed the spectral simulation applying two methods, the Mie formalism for spherical particles[43] and a numerical simulation based on the finite element method (FEM) which included the contribution of substrates using COMSOL MultiPhysics. In the Mie calculation, a concentric spherical Au NP core–polymer shell structure (Figure 4d, inset) dispersed in water was assumed with various shell thicknesses. We assumed the refractive index of the PNIPAM shell as 1.45, that is, slightly smaller than 1.495 of neat polymer[39] because the phase-separated droplet may contain some water, the amount of which is not accessible. We did not consider a smaller value of 1.40 because this value gave shell thickness-dependent LSPR scattering peak shifts much smaller than those observed in the experiments. As shown in Figure 4d, both LSPR scattering spectral redshift and the gradual increase in scattering intensities from the shell were reproduced. According to the Mie simulation, the PNIPAM droplet with diameter 0.7 μm containing a 100-nm-diamter Au NP would give a scattering spectrum similar to the one measured at the laser peak power density of 2.6 mW $\mu m^{-2}$ (compare Figure 4b and 4d).

(a)

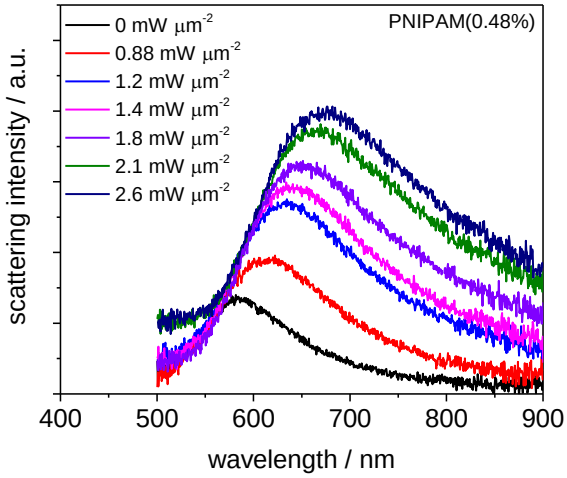
PNIPAM(0.48%)
0 mW μm-2
0.88 mW μm-2
1.2 mW μm-2
1.4 mW μm-2
1.8 mW μm-2
2.1 mW μm-2
2.6 mW μm-2
scattering intensity / a.u.
wavelength / nm

(b)

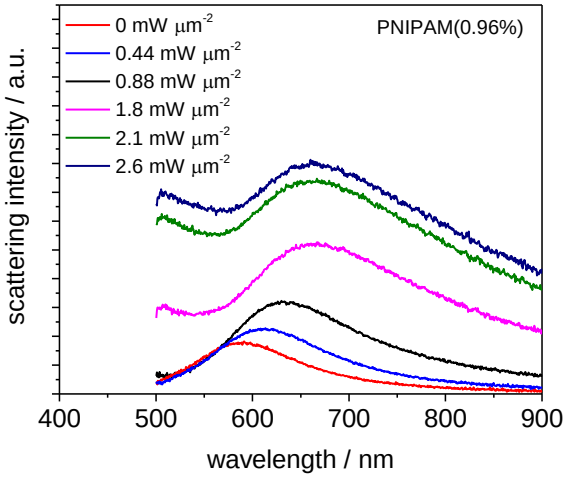
PNIPAM(0.96%)
0 mW μm-2
0.44 mW μm-2
0.88 mW μm-2
1.8 mW μm-2
2.1 mW μm-2
2.6 mW μm-2
scattering intensity / a.u.
wavelength / nm

(c)

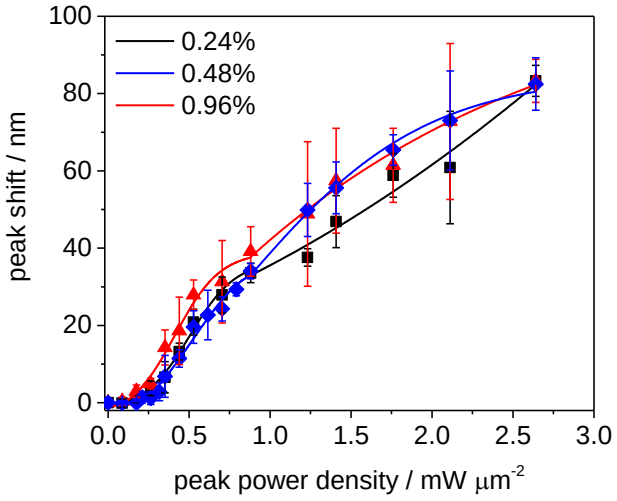
0.24%
0.48%
0.96%
peak shift / nm
peak power density / mW μm-2

(d)

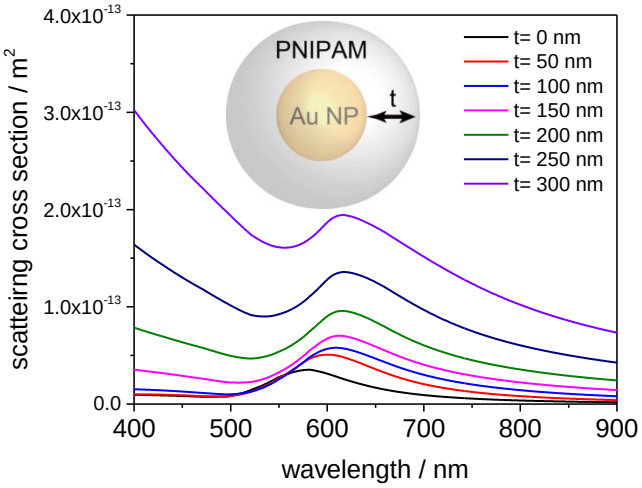
PNIPAM
Au NP
t
t= 0 nm
t= 50 nm
t= 100 nm
t= 150 nm
t= 200 nm
t= 250 nm
t= 300 nm
scatteirng cross section / m2
wavelength / nm

(e)

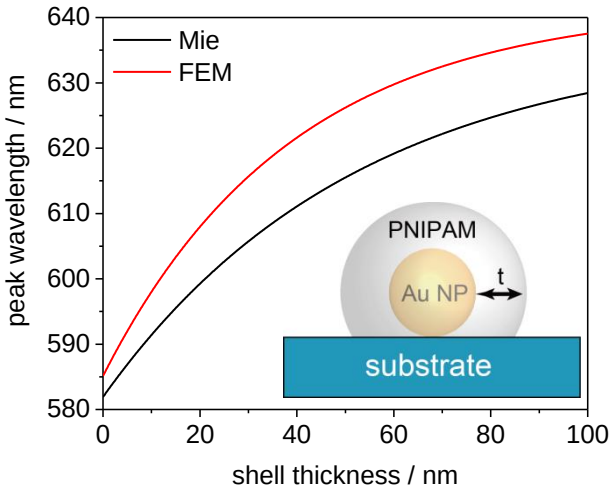
Mie
FEM
PNIPAM
Au NP
t
substrate
peak wavelength / nm
shell thickness / nm

(f)

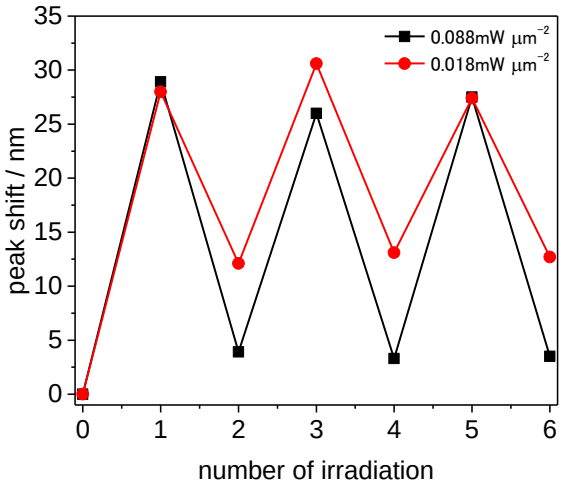
0.088mW μm-2
0.018mW μm-2
peak shift / nm
number of irradiation

**Figure 4**.

(a,b) Light-scattering spectral changes of a 100-nm-diameter Au NP supported on sapphire substrate during illumination as a function of laser peak power density in aqueous 0.48% (a) and 0.96% (b) PNIPAM.

(c) Light-scattering peak shift for a 100-nm-diamter Au NP supported on a sapphire substrate as a function of laser peak power density at three PNIPAM concentrations, 0.24%, 0.48% and 0.96%.

(d) Scatting spectral simulation based on Mie calculation for a concentric core–shell particle consisting of a 100-nm-diameter Au NP with various thicknesses of a shell of n=1.45 nm suspended in water (n=1.33).

(e) Scattering spectral peak as a function of shell thickness simulated based on FEM, considering the effect of a sapphire substrate (n=1.77) in comparison with the Mie calculation for a concentric core–shell particle.

(f) Effect of repeated irradiation with high and low power cycles: 5.3 mW $\mu m^{-2}$ for 2 s (0→1, 2→3, 4→5) and 0.088 or 0.018 mW $\mu m^{-2}$ for 60 s (1→2, 3→4, 5→6), on scattering peak shifts for a 100-nm-diamter Au NP supported on a sapphire substrate.

---

When supported on a sapphire substrate, the droplet diameter was estimated from imaging as 2 μm for irradiation at 5.3 mW $\mu m^{-2}$. Although we could not determine exactly the PNIPAM droplet size at intensities < 5.3 mW $\mu m^{-2}$ from imaging because of difficulty in determining the droplet size distinct from the laser spot, we assumed that the droplet size was smaller than the laser spot of ~1 μm. In contrast, the scattering spectral estimation should be limited to droplet diameters < 1 μm because, for much bigger droplets with greater shell thicknesses, severely distorted scattering spectra can occur owing to the greater scattering contribution from a shell. Thus the darkfield imaging can be more reliably used for estimation of diameters >1 μm.

The FEM calculations were performed to include the substrate effect on the scattering spectra. Figure 4e shows the LSPR spectral peak shift as a function of shell thickness (see Supporting Information S6 for spectra). Inset is the pictorial representation of a configuration for simulation of a Au NP/PNIPAM shell/sapphire exposed to water. For comparison, the results of the Mie calculation are also given. Both the Mie calculation and FEM gave a greater LSPR scattering peak

redshift as a function of shell thickness, up to 100 nm. The numerical simulation including a sapphire substrate, however, gave a slightly greater shift than the simple core–shell model. The numerical simulation gave the spectral shift closer to the experimental ones and may describe the spectra more accurately. However, we found that the FEM computation needs considerable computational time, in particular, for shell thicknesses > 100 nm, far from practical use. A weak point of the simple core–shell model is to neglect the restricted accessible volume for the shell formation in the presence of a substrate. The ratio of inaccessible volume to accessible volume dependent on the shell thickness is calculated on the basis of simple geometric consideration, as given in Supporting Information S6. We concluded that the inaccessible volume, 25% for t=100 nm and 40% for t=500 nm, affects the scattering spectral calculation by the simple core–shell model to a lesser extent, and the spectral simulation in Figure 4d is acceptable.

When we apply laser intensities > 3.7 mW $\mu m^{-2}$ on sapphire, we observed permanent redshift in the LSPR scattering spectra. This was consistent with the darkfield imaging in Figure 2b, in which a particle larger than the original Au NP remained after terminating the illumination. The SEM imaging revealed that Au NPs were encapsulated (Supporting Information S7). However, we found that further illumination at a weak intensity can result in blueshift of the scattering spectrum. Figure 4f shows three repeated cycles of intense (5.3 mW $\mu m^{-2}$, 2s) and weak (0.088 mW $\mu m^{-2}$ or 0.018 mW $\mu m^{-2}$, 60 s) illuminations. We observed the photoswitching behavior for LSPR peak position corresponding to encapsulation and decapsulation. We refer to the mechanism of this behavior in Section 4.

*4. Mechanistic aspect of plasmonic-heating-induced phase separation*

We found that thermoresponsive polymers were attracted to a Au NP under illumination with a wavelength near the LSPR, forming a microdroplet. Here the contribution of optical trapping to the droplet formation should be minor because of moderate focusing at low intensities; instead, the particle heating is primarily responsible. We observed that more and more polymers were pouring into the high-temperature area adjacent to the particle, forming a droplet with increasingly larger diameters as the particle temperature increases. A simple calculation suggested that PNIPAM molecules dissolved in aqueous solution were concentrated into a droplet at least 50 times assuming 50% PNIPAM. The phenomenon observed is unusual because PNIPAM that exhibits a positive thermophoretic mobility, $D_T$, is normally repelled from the high-temperature area through thermophresis.[15] Here the thermoresponsive nature of polymers is responsible for the present observation of a microdomain formed and grown surrounding the hot NP. First, the temperature field around the Au NP acts to hold a droplet because of the temperature gradient that is steeper as being closer to the NP. For the attachment of droplet to Au NP, hydrophobic interaction must be responsible. Second, the LCST-induced phase separation around the hot NP causes the concentration deficiency within the volume near the droplet containing the Au NP, which can promote the diffusion of polymers from the outside area to the droplet. Presumably, the droplet size is determined by a balance between incoming and outgoing rates of diffusing polymers at a given particle temperature.

The phase separation of PNIPAM and PVME around a Au NP was basically reversible for heating/cooling: the droplet was observed only during illumination. This is understandable because LCST behavior of the polymers is reversible.[1,3] Two points, however, should be addressed on the accumulation of polymers after illumination. On glass substrates, permanent accumulation occurred at high laser intensities. Vapor bubble formation around a Au NP is responsible for this permanent accumulation. In pure water, the generation of nano- and microbubbles on CW laser illumination of plasmonic NPs occurred in a superheated water when the particle temperature was raised to

between 220 and 240°C (493–513 K), much higher than the boiling point of water (100°C or 373 K).[16-18] Estimated particle temperatures were 500–600 K. Bubbles have the ability to collect colloids and NPs through Marangoni convection, resulting in fixation of them on substrates.[26-29,35] The present observation of PNIPAM and PVME fixation is consistent with bubble-induced accumulation.

We also observed the fixation of PNIPAM on the sapphire substrate after illumination was stopped, as given in Figure 2b, Figure 4f and Supporting Information, Figure S7. For sapphire, because of its remarkable cooling effect, the particle temperatures during illumination may not be so high to induce vapor bubble generation. We assume that another mechanism can operate. The phase separation of PNIPAM has been thoroughly investigated in bulk aqueous solution and its phase diagram has been established,[3] as given in Supporting Information S8. According to this diagram, as well as the demixing line between one solution phase and two liquid phases, there is a glass transition line in the high concentration region.[45] This line steeply decreases with decreasing PNIPAM concentration, in particular, at temperatures below $T_{BT}$, the vitrification temperature (35°C at 80% PNIPAM). This suggests that if a PNIPAM-rich phase experiences a quick temperature decrease it may undergo a glass transition to a solid-like or gel-like state. We assume that such a glass transition on sapphire substrate can result in the accumulation of the polymers when the illumination is stopped. Interestingly, slight heating again dissolved the polymer deposit (Figure 4f).

The kinetics of phase separation for the thermoresponsive polymers, in particular, at the nanoscale is of extreme interest. For bulk solutions, temperature-jump transient spectroscopy and temperature-jump transient grating methods have been applied to reveal kinetics of phase transition/phase separation for aqueous polymers including PNIPAM and PVME.[46-48] It was found that demixing occurs at the time scale of 10–100 ms with the remixing time of a few seconds. The time resolution of our present measurement is approximately 1 s. However, we observed the time dependent increase/decrease in droplet diameters for the 8.0% PVME solution that has relatively high viscosity. We intend to improve the time resolution in future studies.

Our present finding is that the plasmonic heating of a single Au NP can trap thermoresponsive polymers around the NP, forming a phase-separated droplet. The ability of plasmonic heating to induce migration and accumulation is not limited to thermoresponsive polymers. Molecules like poly(ethylene glycol) and sodium dodecyl sulfate as well as silica colloids were found to accumulate surrounding a hot Au NP after laser illumination.[49] While photothermal bubbles can collect and fix colloids and NPs by promoting thermal and Marangoni convection[29], plasmonic heating manipulates colloids and macromolecules through a similar mechanism at low laser intensities. Plasmonic heating-induced manipulation is a technically benign procedure without the aid of bubbles, but has potential to fabricate small structures if technical sophistication is attained. In this context, the concept of convection-enhanced and temperature-assisted optical trapping has been postulated.[50,51] The practical merits and demerits of plasmonic-heating-induced manipulation over local medium heating and optical trapping are summarized in Table l.

Table 1. Plasmonic-heating-induced *vs*. local medium-heating-induced phase separation.

| paradigm | plasmonic heating | local medium heating | optical trapping |
|---|---|---|---|
| trapping mode | 2D | 3D | 3D |
| laser wavelength | 488 nm | 1064 nm | 1064 nm |
| mechanism | local temperature field | medium heating | optical gradient force |
| peak power density | $10^4$–$10^5$ W cm$^{-2}$ | $10^8$–$10^9$ W cm$^{-2}$ | $10^8$–$10^9$ W cm$^{-2}$ |
| microscopy | darkfield | brightfield | brightfield |
| time evolution | 1–100 s | 10–1000 s | 10–100 s |
| medium | $H_2O$/substrate | $H_2O$ | $D_2O$ |

## Conclusion

We used plasmonic-heating to induce the phase separation of thermoresponsive polymers and demonstrated a 2D trapping of the polymers around a single Au NP supported on a substrate under illumination from a moderately-focused laser beam. 3D extension is possible but the present configuration is convenient for the confinement of the polymers on substrates. We used a 488-nm laser light to excite both LSPR and intraband transitions, resulting in particle heating. The generated temperature field is mainly responsible for trapping thermoresponsive polymers. In optical trapping assisted by a gradient force, however, the particle heating that facilitates Brownian motion needs to be bypassed. Most importantly, our laser power is very low, much less than that used in the direct medium heating or optical trapping experiment. We succeeded in applying darkfield microscopy imaging that has previously not been used for observing phase separation. As a result, we obtained high contrast images. The significant findings of the present study are: (1) the plasmonic heating of a single Au NP with a laser power of ~$10^4$ W $cm^{-2}$ enables a single-domain phase separation around the NP, which is considerably energy saving compared with medium heating-induced microdroplet fabrication using an infrared laser with a power of ~$10^9$ W $cm^{-2}$; (2) by illuminating various intensity of a laser beam on Au nanostructured substrates, the location and size of the droplet is adjustable so that one can separate polymer droplets from the solution at any location; and (3) using a high thermal conductivity sapphire substrate, permanent fixation of the polymers can be attained without the aid of vapor bubbles for further use.

ASSOCIATED CONTENT

Supporting Information

The Supporting Information is available free of charge on the ACS Publications website at DOI: 10.1021/acs.jpcc.7b07187.

Particle image and the corresponding histogram, brightfield images of PNIPAM droplets, diameter of a light scattering sphere as a function of time for PNIPAM, darkfield images of PVME droplets, concentration-dependent viscosity of PVME solution, light scattering spectral simulation, SEM images of Au NPs, phase diagram of thermoresponsive polymer solution, and movie files (AVI) showing growth and collapse of PNIPAM droplets.

AUTHOR INFORMATION

Corresponding Author

Tel.: +81-88-656-7389. E-mail: hashichem@tokushima-u.ac.jp

ORCID

Takayuki Uwada: 0000-0003-4272-7964

Shuichi Hashimoto: 0000-0002-8020-5537

Author contributions

[#] I.A. and J.C. contributed equally to perform optical measurements and analyses. S.H. designed the experiment. T.U. performed a numerical simulation. S.H. prepared the manuscript with contributions from all authors. All authors have given approval to the final version of the manuscript.

Notes

The authors declare no competing financial interest.

ACKNOWLEDGMENTS

Financial support from JSPS KAKENHI (No. 17K05005) and Iketani Science & Technology Foundation (No. 0291052-A) is gratefully acknowledged.

**References**


1. Halperin, A.; Kröger, M.; Winnik, F. M. Poly(*N*-isopropylacrylamide) Phase Diagrams: Fifty Years of Research. *Angew. Chem. Int. Ed*. **2015**, *54*, 15342–15367.
2. Wei, M.; Gao, Y.; Li, X.; Serpe, M. J. Stimuli-responsive Polymers and Their Applications. *Polym. Chem*., **2017**, *8*, 127–143.
3. Aseyev, V. O.; Tenhu, H.; Winnik, F. M. Temperature Dependence of the Colloidal Stability of Neutral Amphiphilic Polymers in Water. *Adv. Polym. Sci*. **2006**, *196*, 1–85.
4. Ishikawa, M; Misawa, H.; Kitamura, N.; Fujisawa, R,; Masuhara, H. Infrared Laser-Induced Photo-Thermal Phase Transition of an Aqueous Poly(*N*-isopropylacrylamide) Solution in the Micrometer Dimension. *Bull. Chem. Soc. Jpn*. **1996**, *69*, 59–66.
5. Hofkens, Y.; Hotta, J.; Sasaki, K.; Masuhara, H.; Iwai, K. Molecular Assembling by the Radiation Pressure of a Focused Laser Beam: Poly(*N*-isopropylacrylamide) in Aqueous Solution. *Langmuir* **1997**, *13*, 414–419.
6. Tsuboi, Y.; Nishino, M.; Matsuo, Y.; Ijiro, K.; Kitamura, N. Phase Separation of Aqueous Poly(vinyl methyl ether) Solutions induced by the Photon Pressure of a Focused Near-Infrared Laser Beam. *Bull. Chem. Soc. Jpn*. **2007**, *80*, 1926–1931.
7. Pan, W.; Kolomeisky, A. B.; Vekilov, P. G. Nucleation of Ordered Solid Phases of Proteins via a Disordered High-density State: Phenomenological Approach. *J. Chem. Phys*. **2005**, *122*, 174905.
8. Katsumoto, Y.; Tsuchiizu, A.; Qiu, X.; Winnik, F. Dissecting the Mechanism of the Heat-Induced Phase Separation and Crystallization of Poly(2-isopropyl-2-oxazoline) in Water through Vibrational Spectroscopy and Molecular Orbital Calculations. *Macromolecules*, **2012**, *45*, 3531–3541.
9. Sugiyama, T.; Masuhara, H. Laser-induced Crystallization and Crystal Growth. *Chem. Asian J*., **2011**, *6*, 2878–2889.
10. Novotny, L.; van Hulst, N. Antennas for Light. *Nature Photon*. **2011**, *5*, 83–90.

11. Le Ru, E. C.; Etchegoin, P. G. *Principles of Surface-Enhanced Raman Spectroscopy*; Elsevier: Amsterdam, 2009.
12. Geddes, C. D. Ed. *Metal-Enhanced Fluorescence*; Wiley: Weinheim, **2010**.
13. Baffou, G.; R. Quidant, R. Thermo-plasmonics: Using Metallic Nanostructures as Nanosources of Heat. *Laser Photonics Rev*., **2013**, *7*, 171–187.
14. Govorov, A. O.; Richardson, H. H. Generating Heat with Metal Nanoparticles. *Nano Today*, **2007**, 2, 30–38.
15. Orlishausen, M.; Köhler, W. Forced Phase Separation by Laser-Heated Gold Nanoparticles in Thermoresponsive Aqueous PNIPAM Polymer Solutions. *J. Phys. Chem. B* **2015**, *119*, 8217−8222.
16. Fang, Z.; Zhen, Y-R.; Neumann, O.; Polman, A.; Garcia de Abajo, F.; Nordlander, P.; Halas, N. J. Evolution of Light Induced Vapor Generation at Liquid-immersed Metallic Nanoparticle. *Nano Lett*. **2013**, *13*, 1736–1742.
17. Baffou, G; Polleux, J.; Rigneault, H.: Monneret, S. Super-Heating and Micro-Bubble Generation around Plasmonic Nanoparticles under cw Illumination. *J. Phys. Chem. C* **2014**, *118*, 4890–4898.
18. Hou, L.; Yorulmaz, M.; Verhart, N. R.; Orrit, M. Explosive Formation and Dynamics of Vapor Nanobubbles around a Continuously Heated Gold Nanosphere. *New. J. Phys*. **2015**, *17*, 013050.
19. Aibara, I.; Mukai, S.; Hashimoto, S. Plasmonic-Heating-Induced Nanoscale Phase Separation of Free Poly(*N*-isopropylacrylamide) Molecules. *J. Phys. Chem. C*, **2016**, *120*, 17745–17752.
20. Honda, M.; Saito, Y.; Smith, N. I.; Fujita, K.; Kawata, S. Nanoscale Heating of Laser Irradiated Single Gold Nanoparticles in Liquid. *Opt. Express* **2011**, *19*, 12375–12383.
21. Karg, M.; Jaber, S.; Hellweg, T.; Mulvaney, P. Surface Plasmon Spectroscopy of Gold-poly-*N*-isopropylacrylamide Core-shell Particles. *Langmuir* **2011**, *27*, 820–827.
22. Kusolkamabot, K.; Sae-ung, P.; Niamnont, N.; Wongravee, K.; Sukwattanasinitt, M.; Hoven, V. P. Poly(*N*‑isopropylacrylamide)-Stabilized Gold Nanoparticles in Combination with Tricationic

Branched Phenylene-Ethynylene Fluorophore for Protein Identification. *Langmuir* **2013**, *29*, 12317–12327.

23. Garcés-Chávez, V.; Quidant, R.; P. J. Reece, P. J.; Badenes, G.; Torner, L.; K. Dholakia, K. Extended Organization of Colloidal Microparticles by Surface Plasmon Polariton Excitation. *Phys. Rev. B*, **2006**, *73*, 085417.
24. Lin, L.; Peng, X.; Wang, M.; Scarabelli, L.; Mao, Z.; Liz-Marzán, L. M.; Becker, M. F.; Zheng, Y. Light-directed Reversible Assembly of Plasmonic Nanoparticles using Plasmon-enhanced Thermophoresis. *ACS Nano*, **2016**, *10*, 9659–9668.
25. Lin, L.; Peng, X.; Wei, X.; Mao, Z.; Xie, C.; Zheng, Y. Thermophoretic Tweezers for Low-power and Versatile Manipulation of Biological Cells. *ACS Nano*, **2017**, *11*, 3147–3154.
26. Zheng, Y.; Liu, H.; Wang, Y.; Zhu, C.; Wang, S.; Cao, J.; Zhu, S. Accumulating Microparticles and Direct-writing Micropatterns using a Continuous-wave Laser-induced Vapor Bubble. *Lab Chip*, **2011**, *11*, 3816–3820.
27. Fujii, S.; Kanaizuka, K.; Toyabe, S.; Kobayashi, K.; Muneyuki,E.; Haga, M. Fabrication and Placement of a Ring Structure of Nanoparticles by a Laser-Induced Micronanobubble on a Gold Surface. *Langmuir*, **2011**, *27*, 8605–8610.
28. Lin, L.; Peng, X.; Mao, Z.; Li, W.; Yogeesh, M. N.; Rajeeva, B. B.; Perillo, E. P.; Dunn, A. K.; Akinwande, D.; Zheng, Y. Bubble-pen Lithography. *Nano Lett.*, **2015**, *16*, 701–708.
29. Xie, Y.; Zhao, C. An Optothermally Generated Surface Bubble and its Applications. *Nanoscale*, **2017**, *9*, 6622–6631.
30. Setoura, K.; Okada, Y.; Werner, D.; Hashimoto, S. Observation of Nanoscale Cooling Effects by Substrates and the Surrounding Media for Single Gold Nanoparticles under CW-Laser Illumination. *ACS Nano*, **2013**, *7*, 7874–7885.
31. Carlson, M. T.; Khan, A.; Richardson, H. H.; Local Temperature Determination of Optically Excited Nanoparticles and Nanodots. *Nano Lett.*, **2011**, *11*, 1061–1069.
32. Brongersma, M. L.; Halas, N. J.; Nordlander, P. Plasmon-induced Hot Carrier Science and

Technology. *Nat. Nanotechnol.*, **2015**, 10, 25–34.

33. Keblinski, P.; Cahill, D. G.; Bodapati, A.; Sullivan, C. R.; Taton, T. A. Limits of Localized Heating by Electromagnetically Excited Nanoparticles. *J. Appl. Phys.*, **2006**, *100*, 054305.
34. Marchand, A.; Weijs, J. H.; Snoeijer, J. H.; Andreotti, B. Why is Surface Tension a Force Parallel to the Interface? *Am. J. Phys*. **2011**, *79*, 999–1008.
35. Setoura, K.; Ito, S.; Miyasaka, H. Stationary Bubble Formation and Marangoni Convection induced by CW laser Heating of a Single Gold Nanoparticle. *Nanoscale*, **2017**, *9*, 719–730.
36. Balu, C.; Delsanti, M.; Guenoun, P. Colloidal Phase Separation of Concentrated PNIPAm Solutions. *Langmuir*, **2007**, *23*, 2404–2407.
37. Xue, N.; Qiu, X-P.; Aseyev, V.; Winnik, F. M. Nonequilibrium Liquid−Liquid Phase Separation of Poly(*N*‑isopropylacrylamide) in Water/Methanol Mixtures. *Macromolecules* **2017**, *50*, 4446−4453.
38. Meier-Koll, A.; Pipich, V.; Busch, P.; Papadakis, C. M.; Müller-Buschbauma, P. Phase Separation in Semidilute Aqueous Poly(*N*-isopropylacrylamide) Solutions. *Langmuir*, **2012**, 28, 8791−8798.
39. Philipp, M.; Aleksandrova, R.; Müller, U.; Ostermeyer, M.; Sanctuary, R,; Müller-Buschbauma, P.; Krüger, J. K. Molecular versus Macroscopic Perspective on the Demixing Ttransition of Aqueous PNIPAM Solutions by Studying the Dual Character of the Refractive Iindex. *Soft Matter*, **2014**, *10*, 7297–7305.
40. Horne, R. A.; Almeida, J. P.; Day, A. F.; Yu, N. T. Macromolecule Hydration and the Effect of Solutes on the Cloud Point of Aqueous Solutions of Polyvinyl Methyl Ether: A Possible Denaturation and Temperature Control in Homeothermic Animals. *J. Colloid Interface Sci*. **1971**, *35*, 77–84.
41. Meeussen, F.; Bauwens, Y.; Moerkerke, R.; Nies, E.; Berghmans, H. Molecular Complexes Formation in the System Poly(vinyl methyl ether)/water. *Polymer*, **2000**, *41*, 3733–3743.
42. Spevacek, J.; Hanykova, L.; Labuta, J. Behavior of Water during Temperature-Induced Phase

Separation in Poly(vinyl methyl ether) Aqueous Solutions. NMR and Optical Microscopy Study. *Macromolecules* **2011**, *44*, 2149−2153.

43. Zhang, W. Z.; Chen, X. D.; Luo, W.; Yang, J.; Zhang, M. Q.; Zhu, F. M. Study of Phase Separation of Poly(vinyl methyl ether) Aqueous Solutions with Rayleigh Scattering Technique. *Macromolecuels*, **2009**, *42*, 1720–1725.
44. Bohren, C. F.; Huffman, D. R. *Absorption and Scattering of Light by Small Particles*; Wiley: New York, **1983**.
45. Van Durme, K.; Van Assche, G.; Van Mele, B. Kinetics of Demixing and Remixing in Poly(*N*-isopropylacrylamide)/water Studied by Modulated Temperature DSC. *Macromolecules* **2004**, 37, 9596–9605.
46. Tsuboi, Y.; Yoshida, Y.; Okada, K.; Kitamura, N. Phase Separation Dynamics of Aqueous Solutions of Thermoresponsive Polymers Studied by a Laser T-Jump Technique. *J. Phys. Chem. B*, **2008**, 112, 2562-2565.
47. Tsuboi, Y.; Tada, T.; Shoji, T.; Kitamura, N. Phase-Separation Dynamics of Aqueous Poly(*N* -isopropylacrylamide) Solutions: Characteristic Behavior of the Molecular Weight and Concentration Dependences. *Macromol. Chem. Phys*. **2012**, *213*, 1879−1884.
48. Inoue, H.; Kuwahara, S.; Katayama, K. The Whole Process of Phase Transition and Relaxation of Poly(*N*-isopropylacrylamide) Aqueous Solution. *Phys. Chem. Chem. Phys*. **2013**, 15, 3814−3819.
49. Enders, M.; Mukai, S.; Uwada, T.; Hashimoto, S. Plasmonic Nanofabrication through Optical Heating. *J. Phys. Chem. C*, **2016**, *120*, 6723–6732.
50. Bartkiewicz, S.; Miniewicz, A. Whirl-enhanced Continuous Wave Laser Trapping of Particles. *Phys. Chem. Chem. Phys*. **2015**, 17, 1077−1083.
51. Louchev, O. A.; Juodkazis, S.; Murazawa, N.; Wada, S.; Misawa, H. Coupled Laser Molecular Trapping, Cluster Assembly, and Deposition fed by Laser-induced Marangoni Convection. *Opt. Express*, **2008**, 5673−5680.

TOC Graphic

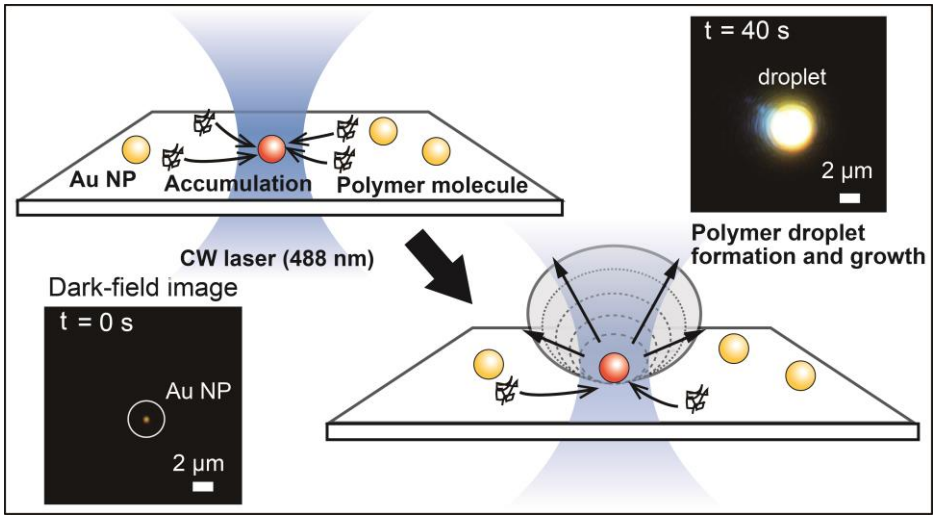
t = 40 s
droplet
2 μm
Au NP
Accumulation
Polymer molecule
CW laser (488 nm)
Polymer droplet
formation and growth
Dark-field image
t = 0 s
Au NP
2 μm